

Entropy generation analysis for the design improvement of a latent heat storage system

*Original*

Entropy generation analysis for the design improvement of a latent heat storage system / Guelpa, Elisa; Sciacovelli, Adriano; Verda, Vittorio. - In: ENERGY. - ISSN 0360-5442. - 54:(2013), pp. 128-138. [10.1016/j.energy.2013.02.017]

*Availability:*

This version is available at: 11583/2520890 since:

*Publisher:*

ELSEVIER

*Published*

DOI:10.1016/j.energy.2013.02.017

*Terms of use:*

This article is made available under terms and conditions as specified in the corresponding bibliographic description in the repository

*Publisher copyright*

(Article begins on next page)

# Entropy generation analysis for the design improvement of a latent heat storage system

Elisa Guelpa, Adriano Sciacovelli<sup>1</sup>, Vittorio Verda

Energy Department - Politecnico di Torino  
ITALY

Phone (+39) 011 564 4478, Fax. (+39) 011 564 4499

e-mail: [adriano.sciacovelli@polito.it](mailto:adriano.sciacovelli@polito.it)

## Abstract

The aim of this work is to investigate design improvements of a shell-and-tube latent heat thermal energy storage unit using an approach based on the analysis of entropy generation. The study is conducted by means of a computational fluid-dynamic (CFD) model which takes into account phase change phenomenon by means of the enthalpy method. Thermal-fluid dynamic problem is solved both for the phase change material (PCM) and heat transfer fluid (HTF). The different contributions to the local entropy generation rate are computed and presented for both un-finned and finned systems. Fin arrangement is then modified according with the analysis of entropy generation distribution in order to increase the efficiency of the system. The results show that the improved system allows to reduce PCM solidification time and increase Second-law efficiency.

The present paper constitutes a first detailed investigation of time evolution of entropy generation occurring during an unsteady process.

## NOMENCLATURE

$A_{mushy}$	Mush zone constant ( $\text{kg m}^{-3} \text{s}^{-1}$ )
$c_p$	Specific heat ( $\text{J kg}^{-1} \text{K}^{-1}$ )
$Ex_{in}$	Exergy flux ( $\text{W K}^{-1}$ )
$\vec{g}$	Gravity acceleration ( $\text{m s}^{-2}$ )
$h$	Specific enthalpy ( $\text{J kg}^{-1}$ )
$h_{ref}$	Reference specific enthalpy ( $\text{J kg}^{-1}$ )
$J_q$	Heat flux ( $\text{W m}^{-2}$ )
$k$	Thermal conductivity ( $\text{W m}^{-1} \text{K}^{-1}$ )
$L$	Specific latent heat ( $\text{J kg}^{-1}$ )
$\dot{m}$	Mass flow rate ( $\text{kg s}^{-1}$ )
$N_s$	Entropy generation number
$p$	Pressure (Pa)
$r$	Radial coordinate (m)
$s$	Specific Entropy ( $\text{J kg}^{-1} \text{K}^{-1}$ )

<sup>1</sup> Corresponding author

$s_p$	Total entropy generation per unit volume ( $\text{W m}^{-3} \text{K}^{-1}$ )
$s_h$	Heat transfer entropy generation per unit volume ( $\text{W m}^{-3} \text{K}^{-1}$ )
$s_\mu$	Fluid friction entropy generation per unit volume ( $\text{W m}^{-3} \text{K}^{-1}$ )
$\vec{S}$	Momentum source term ( $\text{Pa m}^{-1}$ )
$S_p$	Global entropy generation ( $\text{W K}^{-1}$ )
$T$	Temperature (K)
$T_g$	Inlet temperature (K)
$T_0$	Reference temperature (K)
$\vec{v}$	Velocity vector ( $\text{m s}^{-1}$ )
$V$	Volume ( $\text{m}^3$ )
$z$	Axial coordinate (m)
<b>Greek letters</b>	
$\beta$	Thermal expansion coefficient ( $\text{K}^{-1}$ )
$\gamma$	Liquid fraction
$\Delta$	Strain tensor ( $\text{s}^{-1}$ )
$\epsilon$	Computational constant, Eq. (6)
$\eta$	Heat release ratio
$\mu$	Dynamical viscosity (Pa s)
$\rho$	Density ( $\text{kg m}^{-3}$ )
$\vec{\sigma}$	Entropy flux vector ( $\text{W m}^{-2} \text{K}^{-1}$ )
$\tau$	Stress tensor ( $\text{N m}^{-2}$ )
$\Phi$	Heat flux (W)
$\psi$	Second-law efficiency

## 1. Introduction

Imbalance between energy demand and energy supply affects several kind of technologies. Such issue is especially relevant for energy systems; typical examples include solar energy utilization, thermal power generation, combined cooling, heating & power system and air conditioning. As a consequence energy storage plays a fundamental role when it is necessary to fill the gap between energy availability and the need. The most common thermal energy storage technologies are sensible heat storage and latent heat storage. Latent heat thermal energy storage (LHTES) systems have received great attention of several researchers due to their high energy storage density, compactness and the possibility of storing and delivering energy at near constant temperature.

In LHTES units phase change materials (PCM) are utilized which undergo melting or solidification process when energy transfer occurs between the PCM and the working fluid. In the last 25 years various typologies of PCM have been investigated; similarly several geometrical configurations have been studied for the PCM enclosures, such as spherical shell, cylindrical pipes and shell-and-tube configuration. For a comprehensive review of LHTES system applications and PCM distinctive characteristics the reader can refer to papers by Agnè et al. [1] and Zalba et al. [2].

Despite the relative merit of latent heat energy storage the main disadvantage of such technology is related to poor thermal properties of PCMs, in particular low thermal conductivity of phase change materials often leads to unacceptable low melting and solidification rates. As a consequence overall effectiveness of the system is strongly affected. Therefore the advance of LHTES requires the

understanding of thermal behaviour of PCM during the phase transition and the performance assessment of LHTES units.

A great amount of investigations, both numerical and experimental, have been performed to enhance thermal performance of LHTES units and in particular the shell-and-tube configuration since it is closer to real PCM heat exchanger applications. Such configuration is characterized by the PCM filling a cylindrical shell while heat transfer fluid (HTF) flowing through inner tubes and therefore heat transfer takes place between the HTF and the PCM. Several strategies have been proposed to improve thermal performance of LHTES shell-and-tube units including use of high thermal conductivity metal foam [3], encapsulation of the PCM [4] and use of highly conductive PCM-graphite composites [5]. However majority of heat transfer enhancement techniques are based on the use of fins or extended surfaces in order to increase heat transfer area between PCM and HTF. Early investigations were conducted by Choi and Kim [6] who determined heat transfer characteristic for finned and un-finned pipe units during solidification of  $\text{MgCl}_2 \cdot 6\text{H}_2\text{O}$  used as PCM. The authors reported that the ratio of heat transfer coefficient of finned to the un-finned pipe is 3.5 which indicates a significant improvement in thermal performance. Lacroix [7] presented a model based on the enthalpy method for predicting the behaviour of a shell-and-tube LHTES unit. Both finned and bare tubes were considered in the analysis. Several numerical simulations were conducted by the author in order to assess the effect of operating conditions, shell diameter and the presence of fins on the thermal behaviour of the system. The results indicate that radial fins are particularly effective for small HTF inlet temperatures and moderate mass flow rates. Ismail et al. [8] numerically and experimentally analyzed longitudinally finned tubes used in LHTES systems. The proposed numerical model considered heat conduction to be dominant while natural convection in the liquid PCM was neglected. The influence on the phase change process of several design parameters including number of fins, fins length and fin thickness was addressed by means of numerical simulations. Based on experimental and numerical results Ismail et al. [8] pointed out that a tube with five fins of radial length of twice the pipe diameter is the best compromise design in terms of efficiency, heat transfer rate and storage capacity. Ereç et al. [9] investigated thermal energy storage in a shell-and-tube system with a finned tube. The analysis was conducted by mean of a numerical model that considered governing equations for HTF, PCM and pipe wall. The authors performed several numerical simulations to investigate the effect of fin spacing, fin diameter and operating conditions. As expected Ereç et al. [9] concluded that energy storage rate increases with increasing fin diameter and decreasing fin spacing. Agyenim and Hewitt [10] evaluated experimentally the heat transfer characteristics of a longitudinally finned shell-and-tube unit using RT58 a phase change material. Results from the analysis indicate that the use of extended surfaces allows reduce system size of 30%. In addition a 20% increase of HTF inlet temperature brings an increase of 45% of heat transfer coefficient and a 16% reduction of melting time. Recently Ismail and Lino [11] presented the experimental results of the effect of radial fins and turbulence promoters on the phase change process in a latent heat storage system. Tests were conducted on bare tube and finned tube with different fin diameters. Ismail and Lino [11] pointed out that the increase of fin diameter brings a decrease of solidification time and an increase of solidification front velocity. The authors also derived from the experimental results several correlations that can be used for design purposes. Chiu and Martin [12] proposed a design-to-validation protocol for a finned latent heat storage heat exchanger. The author characterized the PCM through the T-history method in order to obtain thermophysical properties of the material. A finite difference model was then used by Chiu and Martin [12] to investigate the design of the heat

exchanger. In particular a parametric study on PCM properties and on fin properties was conducted. The results indicate that fin spacing greatly affects the performance of the system: a one fold increase of melting time is found when fin spacing is doubled.

Performance of engineering devices are directly affected by the thermodynamic irreversibilities associated to transport phenomena such as heat transfer, mass transfer, etc. Entropy generation quantifies thermodynamic irreversibilities which destroy useful energy in a system and directly affect system performance [13]. From this prospective Second-law analysis is more adequate to investigate LHTES systems since the real purpose of thermal storage is to store useful energy, i.e. exergy as pointed out by Bejan [14]. Second-law based performance evaluation of LHTES systems are commonly conducted by means of black-box models or reduced models which do not provide detailed description of the geometry and how thermodynamic irreversibilities are distributed in the system: Bejan [13] investigated a latent heat storage and found optimal melting/solidification temperature which maximize the rate of exergy that can be extracted from PCM. However Bejan [13] considered the system as homogeneous thus no detailed information were obtained about local phenomena in the system. Kousksou et al. [15] developed a model for the analysis and the optimization of cylindrical latent heat storage tank coupled with a solar air heating collector. Both energy and exergy analysis were conducted by the authors in order to understand the behavior of the system. The results show that irreversibilities can be reduced by choosing carefully the melting temperature of the PCM. Ereck and Dincer [16] performed entropy generation and exergy efficiency analysis of a latent heat storage system during charging process. The global entropy generation rate was determined, however the distribution of entropy production within the system was not computed. These authors indicated that entropy generation is crucial for LHTES systems and that it should be carefully considered in order to increase system performance. However the authors did not performed any design improvement on the basis of the entropy generation results. Ezan et al. [17] carried out energy and exergy analyses for the charging period of an ice-on-coil thermal energy storage. Authors developed a numerical model using a thermal resistance network technique in order to investigate heat transfer in the system. They also numerically evaluated energy/exergy effectiveness which indicate that thermal and flow parameters of the heat transfer fluid are the key parameters for determining the performance of the system. However Ezan et al. [17] did not investigated local exergy destruction, i.e. entropy generation within the system. Jegadheeswarana and Pohekar [18] investigated the performance enhancement of a shell and tube storage unit by means of second law analysis. The authors developed a two-dimensional CFD model to solve numerically the phase change problem. The numerical results obtained were used to compute the overall entropy production but no information were given about local distribution of entropy generation rate. Jegadheeswarana and Pohekar [18] pointed out that irreversibilities can be reduced by adding high conductive particles to the PCM but they did not provide further details about performance improvements. MacPhee et al. [19] numerically studied the solidification process in encapsulated ice thermal energy storage system. Both energy and exergy efficiency were evaluated for spherical, cylindrical and slab capsule geometries and different operating conditions. The governing equations were numerically solved by means of a commercial finite-volume code. Authors concluded that considerable increase in performance can be achieved by properly choosing HTF inlet conditions while varying capsule geometry had inconsistent effects on the efficiency depending on the operating conditions. Although they used a CFD model they only computed global entropy generation while no detail about local irreversibilities were investigated.

Although exergy analyses of shell-and-tube LHTES units have been performed by different researchers, literature lacks of Second-law performance evaluation of finned LHTES units as pointed out by Jegadheeswaran et al. [20]. In the authors' knowledge no detailed investigations and design improvements of finned LHTES systems have been performed on the basis of Second-law analysis. In this context the present paper aims at performing a design improvement of a finned shell-and-tube LHTES unit by means of entropy generation analysis. In this work phase change process is numerically study by means of a CFD model that takes into account of the thermo-fluid-dynamic behavior of the system. Temperature, velocity and phase fields are obtained in order to characterize the heat transfer in the system. For the first time a detailed entropy generation analysis of a LHTES unit is performed. In particular, local distribution of entropy production rate is determined and analyzed in order to elucidate the sources of thermodynamic irreversibilities. Design improvements of the system are proposed on the basis of the entropy generation analysis results. Improved fin arrangements which allow to decrease solidification time and increase thermodynamic efficiency of the system are obtained. This works represents a first detailed investigation of the time evolution of entropy generation occurring during an unsteady process. This is particularly important since a clear tendency of many energy systems is the transient operation (e.g. renewable energy systems), therefore design methods should evolve in order to deal with this aspect.

## 2. Mathematical Model

### 2.1 Governing Equations

Figure 1 depicts the system investigated in this paper: it consists of a vertically orientated shell-and-tube LHTES unit. Water is considered as heat transfer fluid and it flows through the inner pipe while phase change material is placed in the space between HTF pipe and the shell. The discharge process of the unit is studied in this work, thus initially liquid PCM at temperature higher than the melting point  $T_m$  fills the shell. At time  $t > 0$  water mass flow rate is allowed to flow through the pipe; inlet temperature  $T_g$  is kept below PCM melting temperature  $T_m$ . As a consequence, heat transfer between HTF and PCM takes place and solidification occurs. The discharge process of the LHTES unit is completed when PCM is completely solid. Both unfinned and finned tubes are considered in this paper; radial fins have an external diameter of 64 mm while different fins distributions are considered as illustrated in the next sections.

For the numerical simulations performed in the paper the energy equation, the continuity equation, and momentum equation are considered. The energy equation for the PCM has been formulated as follow:

$$\frac{\partial}{\partial t}(\rho h) + \nabla \cdot (\rho \vec{V} h) = \nabla \cdot (k \nabla T) \quad (1)$$

where  $\rho$  is the density and  $\vec{V}$  the velocity of the liquid PCM. In order to take into account of PCM phase change the enthalpy-porosity method has been employed [1,21]. Accordingly, the specific enthalpy  $h$  is express as

$$h = h_{ref} + \int_{T_{ref}}^T c_p dT + \gamma L \quad (2)$$

In Eq. (2)  $L$  is the PCM latent heat,  $h_{ref}$  is the enthalpy evaluated at the reference temperature  $T_{ref}$  and  $\gamma$  is known as the liquid fraction and it is defined as follow:

$$\begin{aligned} \gamma &= 0 & \text{if } T < T_{solid} \\ \gamma &= 1 & \text{if } T > T_{liquid} \\ \gamma &= \frac{T - T_{solid}}{T_{liquid} - T_{solid}} & \text{if } T_{solid} < T < T_{liquid} \end{aligned} \quad (3)$$

Density variations due to phase transition have been neglected and Boussinesq approximation is employed. It follows that natural convection in the liquid PCM is taken into account by means of volumetric force term. Consequently continuity and momentum equations here used for the PCM are:

$$\frac{\partial \rho}{\partial t} + \nabla \cdot (\rho \vec{V}) = 0 \quad (4)$$

$$\rho \frac{\partial \vec{V}}{\partial t} + \rho (\vec{V} \cdot \nabla) \vec{V} = -\nabla p + \mu \nabla^2 \vec{V} + \rho \vec{g} (T - T_0) + \vec{S} \quad (5)$$

where  $p$  is the pressure,  $\mu$  is the dynamic viscosity,  $\vec{g}$  is the gravity vector,  $\beta$  is the thermal expansion coefficient,  $T_0$  is the reference temperature and  $\vec{S}$  is the momentum source term.

The enthalpy-porosity formulation treats different phases as porous media by means of the following momentum source term  $\vec{S}$ :

$$\vec{S} = \frac{(1 - \gamma)^2}{(\gamma^3 + \xi)} A_{mushy} \vec{V} \quad (6)$$

where  $A_{mushy}$  is a constant that describes how velocity is reduced to zero when the material solidifies. In this work  $A_{mushy}$  is taken equal to  $10^5 \text{ kg}/(\text{m}^3 \text{ s})$ .

Classical Navier-Stokes equation and energy equation have been used to model the behavior of the HTF. Water flow is considered as laminar, thus no turbulence model is required. Laminar flow represents the worst case scenario concerning heat transfer between PCM and HTF. Indeed an increase of HFT mass flow rate leads to an increase of heat transfer coefficient which contributes to the enhancement of heat transfer between PCM and HTF. Consequently the following analysis and design improvement has been performed considering laminar flow because under such operating condition the impact of fins on heat transfer phenomenon is more relevant. Finally, thermal behavior of the fins is modeled by means of un-steady heat conduction equation.

The PCM here considered is a paraffin wax RT55 produced by RUBITHERM [22]; thermophysical properties are provided by the manufacturer and are reported in Table 1.



## 2.2 Boundary Conditions and Numerical Approach

Initially liquid PCM is considered stationary and at the temperature of 60°C. The base case is characterized by a water inlet temperature of 35°C and a mass flow rate of 28.8 kg/h. Furthermore ambient pressure is imposed on the pipe outlet cross section. Finally the LHTES unit is considered as adiabatic. Three possible fin arrangements are studied in this work, in particular different numbers of fins, fin thickness and fin distributions are considered. Table 2 summarizes all the cases considered in this work.

Finite volume method has been used to numerically solve partial differential equations by means of the commercial code FLUENT. The SIMPLE algorithm has been adopted in order to deal with the pressure-velocity coupling. Furthermore, a 2D axial-symmetric model has been adopted to describe LHTES system geometry. The grid has been systematically refined and a number of about 130000 cells has been found sufficient to ensure grid-independent results: Figure 2 depicts the time evolution of the heat flux in Case II for three different grids; it can be noticed that almost identical results are obtained with grids of 100k and 130k cells, thus the latter has been chosen for the analysis illustrated in the paper. A second order implicit scheme has been employed and the effect of time step has been also addressed; a time step ranging between 0.05 and 0.1 s has been found sufficient to obtain time-step independent solutions. For Case II the effect of time step on solidification time is illustrated in Table 3. It is possible to observe that time step has a minor effect and that the time step chosen for the simulations ensures time independent solutions. Scaled residuals of the variables, including velocity components, mass and temperature have been monitored at each time step to ensure convergence. Specifically the solution has been considered converged when all residual were lower than  $10^{-6}$ . The model adopted in this paper has been validated by the authors against experimental results for LHTES unit and phase change problems. References [23,24] describe validation studies that point out the capability of the model in predicting the behavior of LHTES systems.

## 2.3 First and Second-law analysis

The performance of the LHTES unit have been evaluated on the basis of first law following the approach introduced by Kaizawa et al. [25]. Specifically the heat release ratio has been used as figure of merit. The heat release ratio is defined as the ratio between the total energy released by the unit and the maximum storage capacity of the unit, that is:

$$\eta(t) = \frac{\int_0^t \Phi(t) dt}{\rho_s \cdot L \cdot V + \rho \cdot c_{p,s} \cdot V \cdot (T_i - T_m) + \rho_l \cdot c_{p,l} \cdot V \cdot (T_m - T_g)} \quad (7)$$

where  $\Phi$  is the heat flux exchanged between PCM and HTF,  $V$  is the volume occupied by the PCM and  $T_i$  is the initial PCM temperature.

Beside energy analysis, entropy generation analysis is proposed in order to identify and quantify the various causes of thermodynamic irreversibilities. Design improvement of the LHTES unit are obtained through the analysis of entropy generation rate distribution. The local entropy production can be derived from the transport equation for entropy written for a infinitesimal volume [13,26]:



$$\rho \frac{Ds}{Dt} = -\nabla \cdot \vec{\sigma} + s_p \quad (8)$$

where  $Ds/Dt$  is the substantial derivative of specific entropy  $s$ ,  $\vec{\sigma}$  is the entropy-flux vector and  $s_p$  is the local entropy generation rate. Thermodynamic irreversibilities are due to transport phenomena such as heat transfer, mass transfer, viscous dissipation and chemical reactions [27]. In the problem considered in this paper, i.e. PCM phase change process, entropy generation can be split into two main contributions:

$$s_p = s_h + s_\mu \quad (9)$$

where the first term is the contribution due to fluid friction and the second one is due to heat transfer. Assuming local equilibrium is possible to express  $s_p$  as follow [26-28]:

$$s_p = \underbrace{\frac{-\vec{J}_q \cdot \nabla T}{T}}_{\text{heat transfer}} + \underbrace{\frac{\Delta : \tau}{T}}_{\text{viscous}} \quad (10)$$

where  $\vec{J}_q$  is the heat flux,  $\Delta$  is the strain tensor and  $\tau$  is the stress tensor. The heat flux is obtained by means of Fourier's law:

$$\vec{J}_q = -k\nabla T \quad (11)$$

while strain and stress tensor for a Newtonian incompressible fluid are expressed in the following way:

$$\Delta = \frac{1}{2} \left( \frac{\partial v_i}{\partial x_j} + \frac{\partial v_j}{\partial x_i} \right) \quad (12)$$

$$\tau = \mu \left( \frac{\partial v_i}{\partial x_j} - \frac{\partial v_j}{\partial x_i} \right) \quad (13)$$

The entropy generation over the entire LHTES unit can be immediately obtained by means of integration, that is:

$$S_p = \int s_p dV \quad (14)$$

The integral appearing in the previous equation is extended over the entire LHTES unit illustrated in Fig. 1. Overall system performance are evaluated on the basis of Second-law as follow [16]:

$$\psi = 1 - N_s \quad (15)$$

where the entropy generation number,  $N_s$  is defined as

$$N_s = \frac{T_0 S_p}{Ex_{in}} \quad (16)$$

The denominator of Eq. (15) represents the rate of exergy released by the PCM, that is:

$$Ex_m = \Phi \cdot \left( 1 - \frac{T_0}{T_{PCM}} \right) \quad (17)$$

Equations concerning entropy generation have been implemented in FLUENT by means of User Define Functions (UDFs). Specifically at each time step local gradients of temperature and velocity are computed in order to evaluate local entropy generation rate through Eq. (10). Furthermore global entropy production is obtained by performing numerical integration (Eq. 14) at each instant of time.

From the previous equations it is clear that thermodynamic performance of the system can be globally improved at constant heat flux  $\Phi$  by reducing the entropy generation number. However the entropy generation analysis here introduced allows one to perform a more detailed analysis of the device. From Eq. (10) is possible to analyze and interpret the local distribution of entropy generation and consequently improve LHTES unit configuration in order to reduce local peaks of entropy production and make its distribution more even. Therefore design improvements can be driven by a deeper understanding of local thermodynamic processes and related irreversibilities.

The investigation performed in the paper is a typical thermodynamic analysis since it strongly depends on the concept of entropy production. Entropy generation stems from Second-law of Thermodynamics, therefore the entropy generation analysis is very general and it not restricted to a particular kind of system or process.

## 3. Results

### 3.1 Comparison of finned and un-finned LHTES unit

In this section thermo-fluid-dynamic behavior of LHTES unit with bare pipe and finned pipe are presented and compared. Since different configurations have been analyzed, Case I and Case II reported in Table 1 are initially considered. Both cases are characterized by a water mass flow rate of 28.8 kg/h and an inlet temperature  $T_g = 35^\circ\text{C}$ .

Figure 3 depicts the time evolution of solidification front: in Case I (no fins) solidification initially takes place along the pipe wall because of heat transfer established between HTF and PCM. The amount of solid PCM gradually increases with time until the shell is completely filled by the solidified PCM. It can be noticed from Figure 3 that the solid layer thickness does not vary significantly along the  $z$ -axis. Natural convection currents take place in the shell of the unit: liquid PCM raises along the shell wall while it descends along the cold solid PCM. The solidification process is only slightly affected by buoyancy in the top and bottom portion of the unit. Indeed small variations of solid PCM thickness can be observed in Figure 3. Therefore PCM solidification is mainly dominated by heat conduction, because solid PCM layer progressively increases around the HTF pipe and the corresponding thermal resistance also increases. A similar situation takes place when radial fins are considered: solidification starts along the fins and pipe walls, consequently the solidification front assumes a wavy shape as can be appreciated from Figure 3. Fins enhance the solidification process since, at a given time, the amount of solid PCM is larger for Case II than for Case I. Such effect is more marked for late solidification stage as can be seen from the last contour of Figure 3.

The average heat flux exchanged between HTF and PCM is shown in Figure 4 left. In both cases the initial heat flux is very large then it decreases with time. The heat transfer enhancement due to fins can be clearly seen from Figure 4 left, indeed heat flux is larger for Case II until solidification is complete. As a consequence, finned LHTES unit is preferred as can be also concluded from the time evolution of heat release ratio  $\eta$  reported in Figure 4 right. It can be appreciated that  $\eta$  at any time is larger for Case II, indicating a faster solidification rate and therefore better performance accordingly to energy analysis. Solidification time is reduced of about 15% when radial fins are used.

Finned and un-finned units have been investigated also according with the Second-law analysis. Figure 5 left depicts the time evolution of global entropy generation within the system. Viscous entropy generation is negligible compared to heat transfer entropy production because flow field in the unit is laminar and therefore viscous stresses are small. Consequently the second term on the right hand side of Eq. (10) is not relevant. It is important to stress that, when fins are introduced, entropy production is larger because the enhanced heat transfer induces larger thermal irreversibilities. The average heat flux is larger, therefore the exergy rate released by the PCM increases. As a result, the entropy generation number  $N_s$  diminishes when fins are introduced. In particular time-averaged value of  $N_s$  is reduced of about 5% for Case II in comparison to Case I.

A better understanding of the origin of thermodynamic irreversibility can be achieved by investigating the distribution of local entropy production. Figure 6 depicts the entropy generation due to heat transfer at different times. For both cases at the beginning of the solidification process entropy production is mainly localized within the HTF pipe and in particular along the tube wall. Furthermore larger entropy production can be observed near the outlet section of the pipe. Such distribution of  $s_h$  can be understood by observing the temperature contours reported in Figure 7: thermal boundary layer initially develops along the pipe wall, therefore in such region large temperature gradients are found. Moreover, temperature is lower on the water side, therefore large entropy generation due to heat transfer is observed. In the un-finned LHTES unit,  $s_h$  is also relevant on the PCM side: since heat transfer is established between PCM and HTF, temperature gradients are observed near the pipe wall on the PCM side, thus entropy generation is observed in this region. For Case II, heat flux is mainly exchanged through the fin surface. At  $t = 1000$  s  $s_h$  is not relevant near the tube wall on the PCM side while it is mainly localized near the fins.

As solidification progresses, the entropy generation becomes relevant in most part of the shell, in particular  $s_h$  is predominant where PCM is already solid. Indeed  $s_h$  distribution assumes a shape similar to the solidification front illustrated in Figure 3. It is interesting to notice that at  $t = 10^4$  s a local minimum of  $s_h$  is found near fin roots while entropy generation remains relevant between fins. Thus the presence of radial fins determines a local reduction of the entropy generation. Furthermore from Figure 6 it is also possible to notice that entropy production is more relevant in the upper region of the system, especially for late stage of the solidification process.

### 3.1 Effect of number of fins

The analysis of the local distribution of the entropy generation rate can be used to improve the LHTES unit geometry and in particular the fin arrangement. Accordingly to Eqs. (15) and (16) system performance can be improved by modifying its design in order to reduce the entropy generation number  $N_s$ . This goal can be achieved by reducing entropy generation without penalizing the rate of exergy released by the PCM. However, a second situation may occur: an increase of

entropy production is not necessary a drawback if it is accompanied by a sufficient increase of exergy flux and a consequent decrease of  $N_s$ . The design should tend to make the local entropy production distribution more homogeneous as possible, without necessarily minimizing it. In order to consider comparable cases in the following analysis total volume occupied by fins is considered as constant. Therefore the maximum energy that can be stored in the unit is the same for all the cases.

According with the previous results, the upper part of the LHTES unit and the region between two fins are the points where entropy generation is larger and where geometry changes are more appropriate. The first design improvement of the finned unit consists in halving the axial distance between two radial fins. Consequently, the first improved design (Case III) consists in a LHTES unit with 27 fins which thickness is reduced by half compared to the initial finned configuration (Case II). In Figure 8, entropy generation distributions in the new LHTES unit and in the original finned configuration are compared. Some improvements can be observed: at the beginning of the solidification process, i.e.  $t = 3000$  s, the extent of the high entropy generation region near the pipe is slightly reduced when a more dense fin distribution is considered. Though the effect is not particularly marked since at early times solidification takes place mainly along the outer surface of the pipe. However major differences can be observed at  $t = 10^4$  s since at this stage solidification occurs along the entire surface of the fins and therefore the effect of the new configuration on the local entropy generation is more clear. In Case III smaller entropy production can be observed in the region between the fins, furthermore thermodynamic irreversibilities are also reduced near the pipe surface in comparison to the original LHTES unit configuration. Moreover, when more fins are introduced, entropy production is also reduced in the upper part of the system as can be noticed from Figure 8 at axial coordinate  $z = 0.85$  m. The new fin arrangement allows one to improve the LHTES unit performance: solidification time is reduced of 16% for Case III in comparison to Case II. Time-averaged value of  $N_s$  is about 0.2 for both Case III and Case II, therefore Second-law performances are similar, although heat transfer is enhanced for Case III since solidification time is reduced. This means that global entropy generation  $S_p$  is higher for Case III but also exergy flux  $Ex_{in}$  is augmented.

### 3.2 Effect of fin distribution

A second step in the LHTES unit design improvement consists in modifying the fins axial distribution along the HTF pipe. It can be noticed from Figure 8 that the upper part of the system remains the most critical one also in Case III. In particular, it can be observed that entropy generation is still relevant near the top of the LHTES unit especially during the late stage of PCM solidification. Therefore, in order to further improve the performance of the system, the possibility of using a non-uniform axial distribution of fins is proposed. In particular a more dense fin distribution in upper region is here adopted while the same number and thickness of fins of Case III have been employed. Specifically, a fin spacing contraction factor  $C_f$  of 0.975 has been used, that is the ratio between any two subsequent fin spacing is equal to 0.975. As a result, more fins are found in the upper part of the LHTES unit.

Figure 9 illustrates how local entropy generation due to heat transfer is affected by the non-uniform fins distribution (Case IV). Although no particular differences can be noticed at the beginning of the solidification process, for time larger than  $10^4$  s it can be observed that entropy production is more homogeneously distributed for Case IV, in particular  $s_h$  is reduced in the region above axial

coordinate  $z = 0.6$  m. Thus the fin distribution adopted for Case IV allows one to improve Second-law performance of the LHTES unit, indeed time-averaged value of  $N_s$  decreases of 17% for Case IV in comparison to Case III.

Figure 10 shows time-wise evolution of heat release ratio  $\eta$  and entropy generation number  $N_s$  for the three fin arrangements considered in this paper. It is clear from the evolution of  $\eta$  that a larger number of fins allows a faster discharge of the LHTES unit, however heat release ratio is not particularly affected by the fin distribution along the HTF pipe. Indeed heat release ratio is almost identical at any time for Case III and Case IV. On the other hand, entropy generation number  $N_s$  and therefore Second-law performance are significantly affected by the way fins are distributed along the LHTES unit. From Figure 10 it is possible to appreciate that  $N_s$  is smaller for Case IV especially during late stage of solidification process. Then a non-uniform distribution of a fins allows to improve Second-law efficiency and also decrease the solidification time, enabling a faster and more efficient discharge of the unit.

Finally Figure 11 depicts time averaged values of Second-law efficiency and global entropy generation per unit volume for Case II, III and IV. It is interesting to notice that when a larger number of fins are considered, that is in Case III and Case IV, the global entropy generation increases compared to Case II. As indicated previously, larger thermodynamic irreversibilities are not necessarily a disadvantage. In fact it is possible to observe from Fig. 11 right that Second-law efficiency is larger for Case III which also presents the larger of global entropy production.

## 5. Conclusions

In this paper, a Second-law analysis of a shell-and-tube latent heat thermal storage unit has been performed. The analysis of the solidification process has been conducted by means of a CFD model that takes into account of the phase change problem through the enthalpy method. The model has been used to compute the thermodynamic irreversibilities associated to fluid friction and heat transfer. Furthermore the analysis of local entropy generation has been used in order to improve LHTES unit performances through the use of radial fins.

The analysis shows that entropy generation due to fluid friction is always negligible compared to heat transfer entropy production and therefore the latter must be considered in order to improve the performance of the unit. Furthermore the analysis shows that the region between two fins and the upper part of the LHTES unit are the points where entropy generation is locally higher and therefore where geometry changes are more proper. In order to improve the system performance two design modifications have been considered: an increase of number of fins and a non-uniform distribution of fins along the heat transfer fluid pipe with the constrain of constant volume occupied by the fins. The results indicate that doubling the number of fins which thickness is reduced by half compared to the initial configuration allows to obtain a more uniform distribution of local entropy generation. As a result solidification time decreases of 16% compared to the original fins configuration. Global entropy generation increases when the number of fins is increased because of the enhanced heat transfer between PCM and HTF. However Second-law efficiency is unaffected since also exergy flux also increases when a large number of fins is considered.

Solidification time is not affected by the axial distribution of fins. However a more dense distribution of fins in the upper part of the LHTES unit allows to obtain an increase of 5% in Second law efficiency. The time evolution of entropy generation number shows that a non-uniform distribution of fins is particularly effective during the late stage of the solidification process when

the remaining liquid PCM is located in the upper region of the LHTES unit. As a result, the time averaged value of entropy generation number decreases of 17%.

In conclusion, this paper shows that entropy generation analysis can be effectively used for the design improvement of advanced thermal storage systems. This analysis must be performed in transient conditions, which is a novelty proposed here. The application highlights that there are critical parts of the process, occurring in specific moments, that should be improved first. Effective changes in the design should be performed in order to improve the performances in these moments. The entropy generation analysis allows one to capture opportunities for performance improvement, therefore this tool is shown to be effective even in the case of transient operation of energy systems. This is an important result, since there is a clear tendency in various modern energy systems towards transient operation.

## References

1. Agyenim, F., Hewitt, N., Eames, P., Smyth, M. A review of materials, heat transfer and phase change problem formulation for latent heat thermal energy storage systems (LHTESS), Renewable and sustainable Energy Reviews 2010; 14: 615-628
2. Zalba B., Marin J. M., Cabeza L. F., Mehling H. Review on thermal energy storage with phase change: materials, heat transfer analysis and applications. Applied Thermal Engineering 2003; 23:251-283.
3. Mesalhy O., Lafdi K., Elgafy A., Keith Bowman K. Numerical study for enhancing the thermal conductivity of phase change material (PCM) storage using high thermal conductivity porous matrix. Energy Conversion and Management 2005; 46: 847-867.
4. A. Sari, C. Alkan, A. Karaipekli, O. Uzun, Microencapsulated n-octacosane as phase change material for thermal energy storage, Solar Energy 2009; 83: 1757-1763.
5. Cabeza L.F., Mehling H., Hiebler S., Ziegler F. Heat transfer enhancement in water when used as PCM in thermal energy storage. Applied Thermal Engineering 2002; 22:1141-1151.
6. Choi J.C., Kim S.D. Heat transfer characteristics of a latent heat storage system using  $MgCl_2 \cdot 6H_2O$ . Energy 1992; 17: 1153-1164.
7. Lacroix M. Study of the heat transfer behavior of a latent heat thermal energy storage unit with a finned tube. International Journal of Heat and Mass Transfer 1993; 36: 2083-2092.
8. Ismail K.A.R., Alves C.L.F., Modesto M.S. Numerical and experimental study on the solidification of PCM around a vertical axially finned isothermal cylinder. Applied Thermal Engineering 2001; 21: 53-77.
9. Erek A., Ilken Z., Acar M.A. Experimental and numerical investigation of thermal energy storage with a finned tube. International Journal of Energy Research 2005; 29: 283-301.



10. Agyenim F., Hewitt N. The development of a finned phase change material (PCM) storage system to take advantage of off-peak electricity tariff for improvement in cost of heat pump operation. *Energy and Buildings* 2010; 42: 1552–1560.
11. Ismail K.A.R, Lino F.A.M. Fins and turbulence promoters for heat transfer in latent heat storage systems. *Experimental Thermal and Fluid Science* 2011; 35: 1010–1018.
12. Chiu J., Martin V. Submerged finned heat exchanger latent heat storage design and its experimental verification. *Applied Energy* 2012; 93: 507-516.
13. Bejan A. Entropy generation minimization. Boca Raton: CRC; 1996.
14. Bejan A. Two thermodynamic optima in the design of sensible heat units for energy storage. *J Heat Transfer* 1978;100:708–12.
15. Kousksou T., F. Strub F., Lasvignottes J.C., Jamil A., Bedecarrats J.P. Second law analysis of latent thermal storage for solar system. *Solar Energy Materials & Solar Cells* 2007; 91:1275–1281.
16. Ereǵ A., Dincer I. An approach to entropy analysis of a latent heat storage module. *International Journal of Thermal Sciences* 2008; 47: 1077–1085.
17. Ezan M. A., Ereǵ A., Dincer I. Energy and exergy analyses of an ice-on-coil thermal energy storage system. *Energy* 2011; 36: 6375-6386.
18. Jegadheeswarana S., Pohekar S.D. Exergy analysis of particle dispersed latent heat thermal storage system for solar water heaters. *Journal of Renewable Sustainable Energy* 2010; 2.
19. David MacPhee D., Ibrahim Dincer I., Beyene A. Numerical simulation and exergetic performance assessment of charging process in encapsulated ice thermal energy storage system. *Energy* 2012, 41: 491-498.
20. S. Jegadheeswaran S., Pohekar S.D., Kousksou T. Exergy based performance evaluation of latent heat thermal storage system: A review. *Renewable and Sustainable Energy Reviews* 2010; 14:2580–2595.
21. Voller V.R., Prakash C. A fixed grid numerical modeling methodology for convection-diffusion mushy region phase-change problems. *International Journal of Heat and Mass Transfer* 1987; 30: 1709-1719.
22. RUBITHERM® (2012). <http://www.rubitherm.de/english/index.htm>
23. Sciacovelli A, Verda V, Colella F. Numerical model for storage systems based on phase change materials. Proceedings of IMECE '11: 2011 ASME International Mechanical Engineering Congress & Exposition. Denver, Colorado, November 11-17, 2011.
24. Sciacovelli A, Verda V. Numerical analysis on melting in a cylindrical heat storage capsule. THERMACOMP 2011, Second International Conference on Computational Methods for Thermal Problems. Dalian, China, September 5-7, 2011.



25. Kaizawa A., Kamano H., Kawai A., Jozuka T., Senda T., Maruoka N. Thermal and flow behaviors in heat transportation container using phase change material. *Energy Conversion and Management* 2008; 49: 698–706.
26. Hirschfelder J.O., Curtiss C.F, Bird R.B. *Molecular theory of gases and liquids*. New York: Wiley; 1954.
27. De Groot S.R., Mazur P. *Non-equilibrium thermodynamics*. New York: Dover Publications; 2011.
28. Sciacovelli A., Verda V. Entropy generation analysis in a monolithic-type solid oxide fuel cell (SOFC). *Energy* 2009; 34: 850–865.
29. Jones BJ, Sun B, Krishnan S, Garimella SV. Experimental and numerical investigation of melting in a cylinder. *International Journal of Heat and Mass Transfer* 2006; 49:2724-38.

### List of Tables

Table 1. Thermophysical properties of the PCM (RT55) [22].

Table 2. Computational cases studied.

Table 3. Results from time step independence analysis.

### List of Figures

Figure 1. LHTES system geometry.

Figure 2. Average heat flux for grid independence test.

Figure 3. Contours of liquid fraction; Case I and Case II.

Figure 4. Left) Average heat flux. Right) Heat release ratio  $\eta$ . Case I and Case II.

Figure 5. Left) Global entropy generation. Right) Entropy generation number  $N_s$ . Case I and Case II.

Figure 6. Entropy generation due to heat transfer. Case I and Case II.

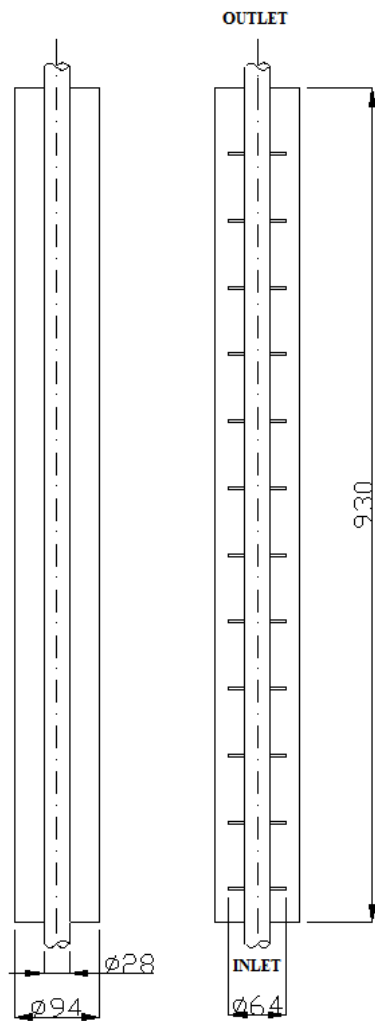
Figure 7. Temperature distribution in the HTF and PCM region. Case I and Case II.

Figure 8. Entropy generation due to heat transfer. Case II and Case III.

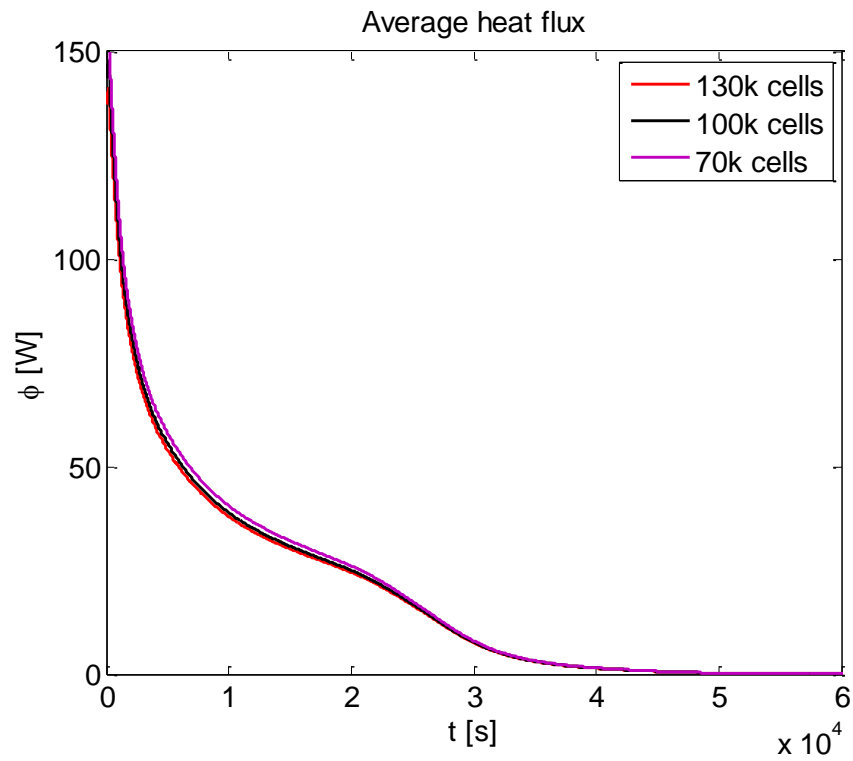
Figure 9. Entropy generation due to heat transfer. Case III and Case IV.

Figure 10. Left) Heat release ratio  $\eta$ . Right) Entropy generation number  $N_s$ . Case II, III and IV.

Figure 11. Left) Global entropy generation. Right) Second-law efficiency.



**Figure 1. LHTES system geometry.**



**Figure 2. Average heat flux for grid independence test.**

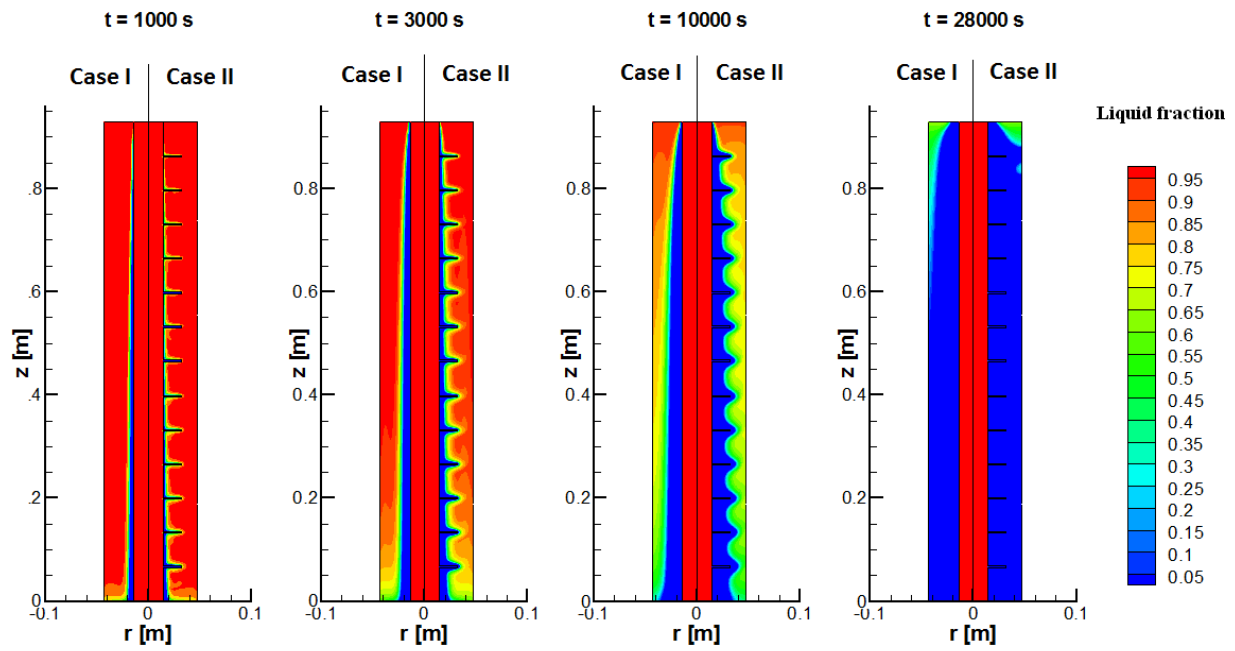


**Figure 3. Contours of liquid fraction; Case I and Case II.**

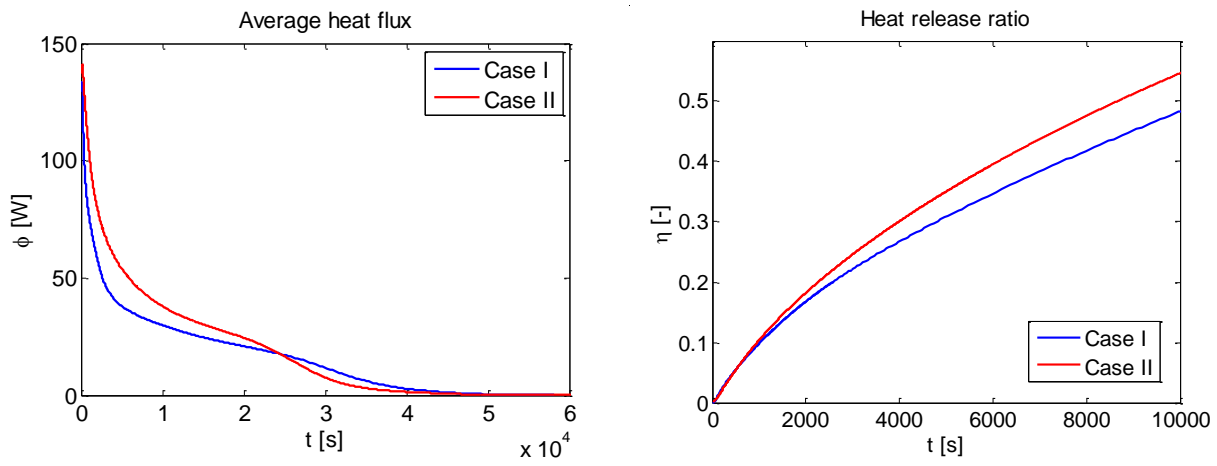


**Figure 4. Left) Average heat flux. Right) Heat release ratio  $\eta$ . Case I and Case II.**

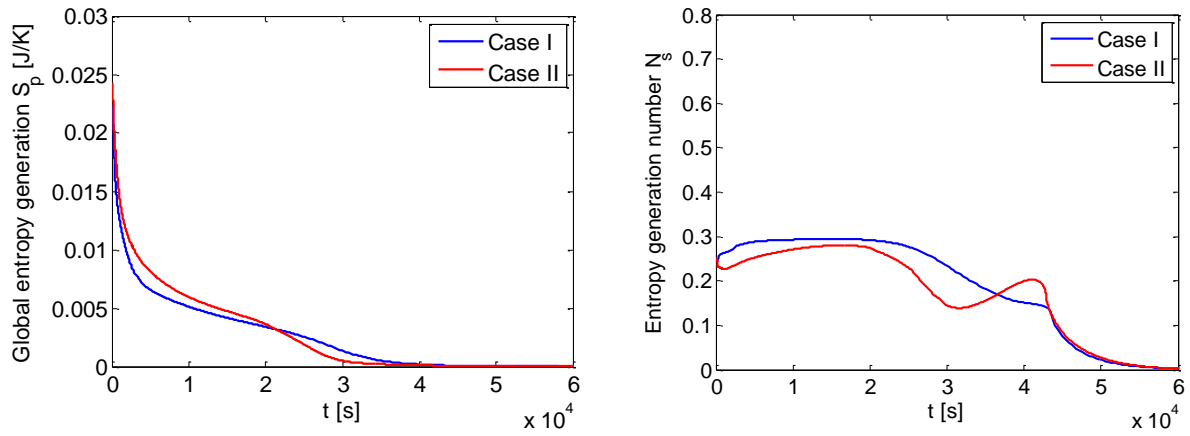


**Figure 5. Left) Global entropy generation. Right) Entropy generation number  $N_s$ . Case I and Case II.**

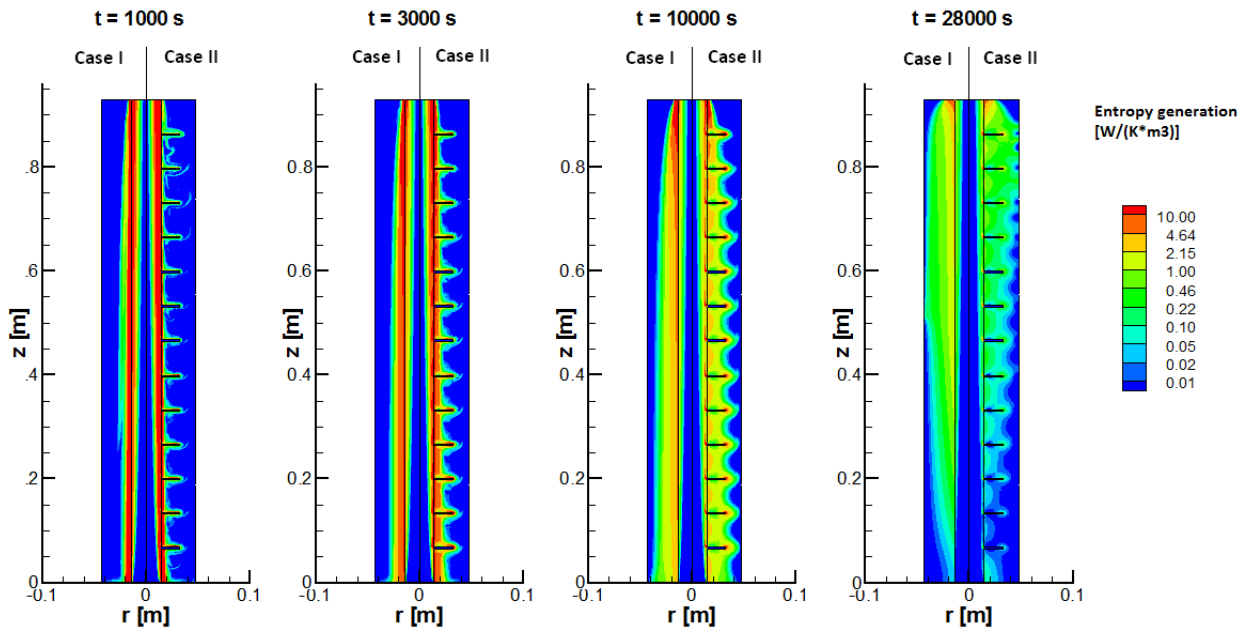


**Figure 6. Entropy generation due to heat transfer. Case I and Case II.**



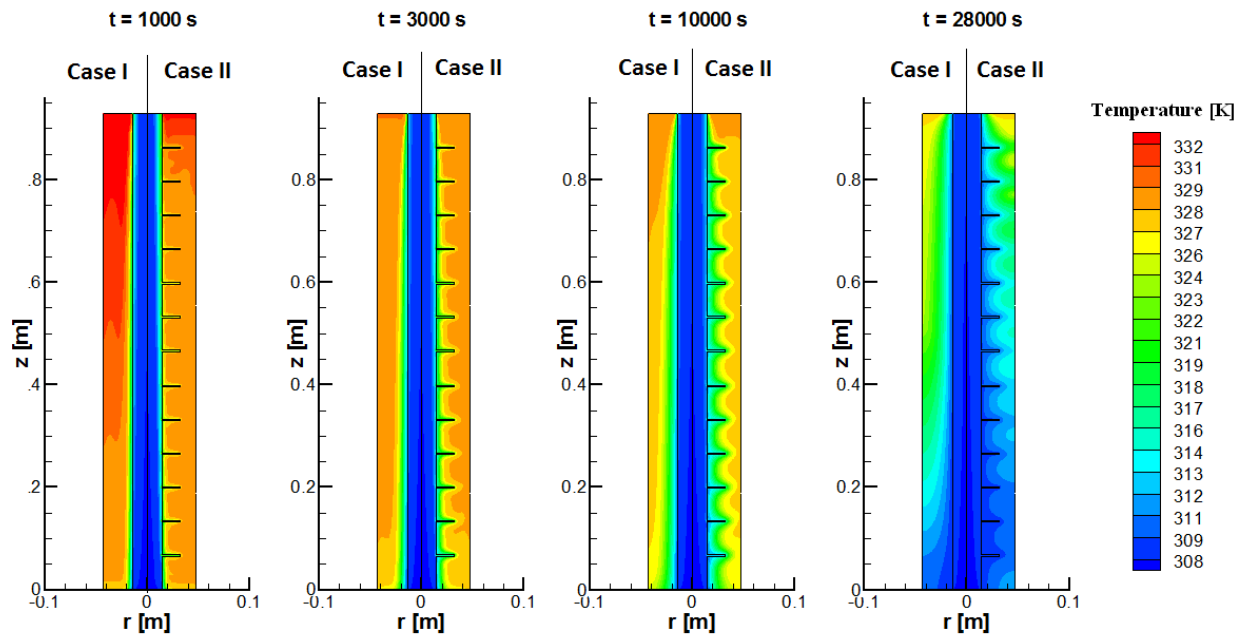


**Figure 7. Temperature distribution in the HTF and PCM region. Case I and Case II.**

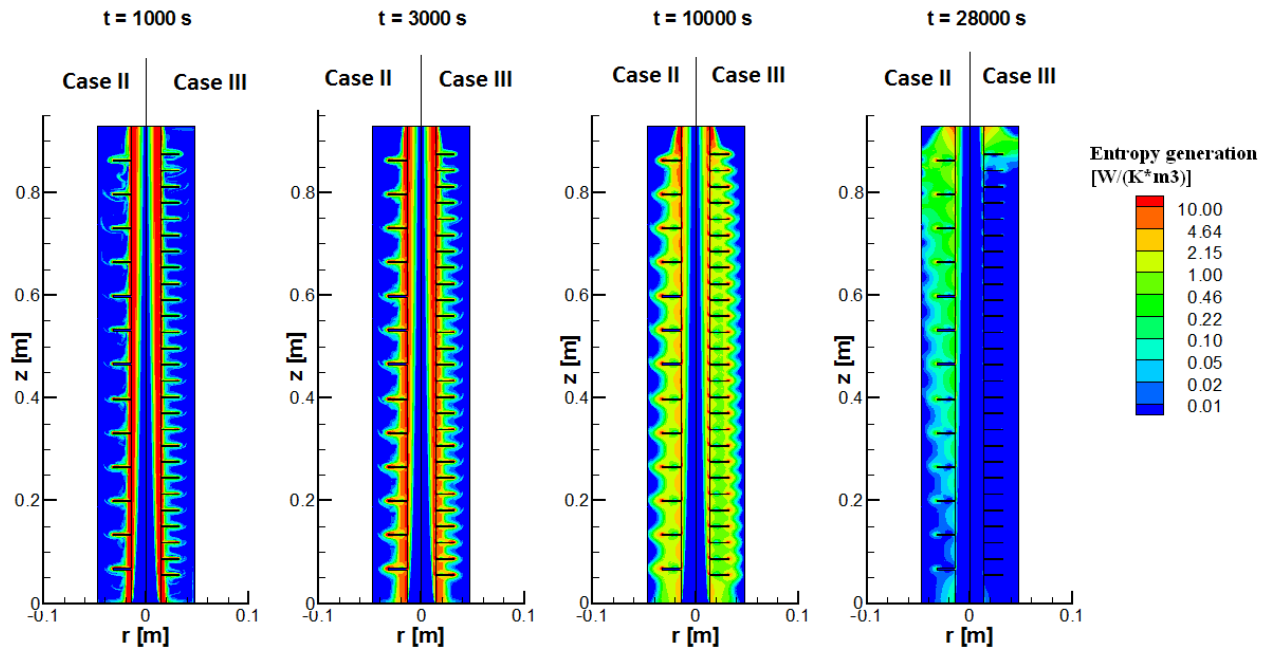


**Figure 8. Entropy generation due to heat transfer. Case II and Case III.**

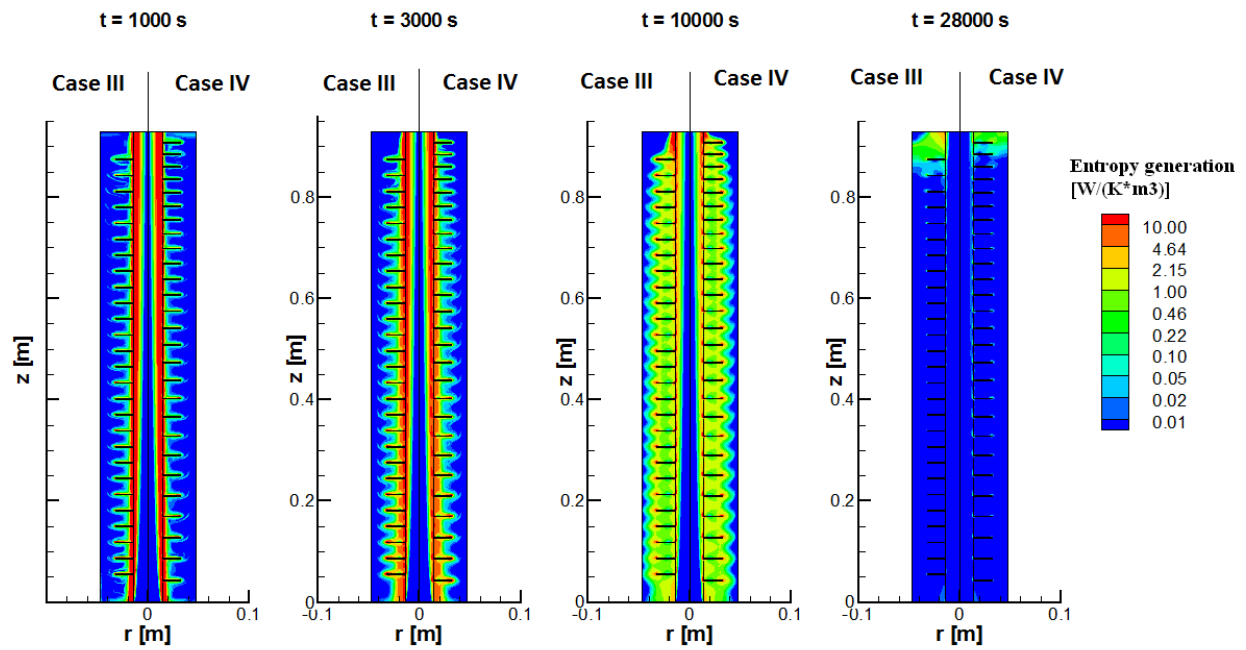
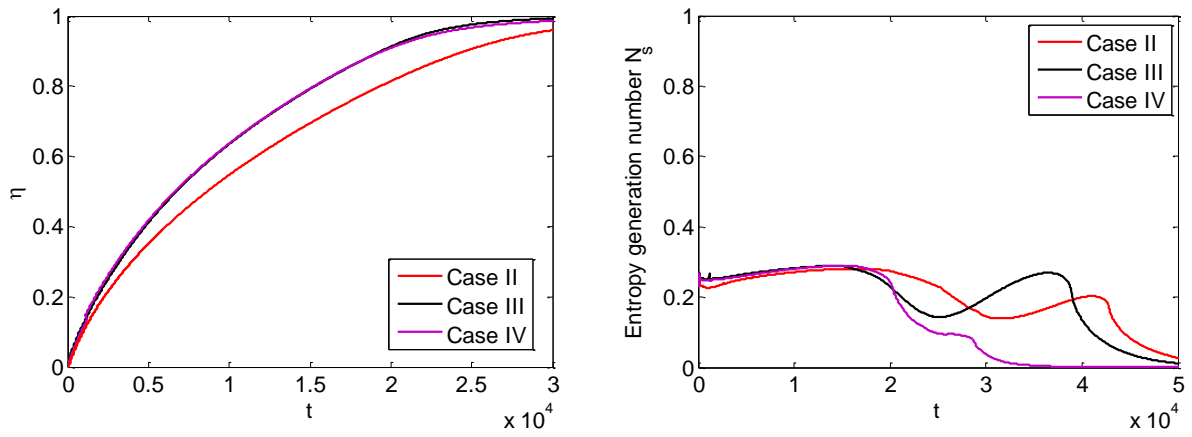
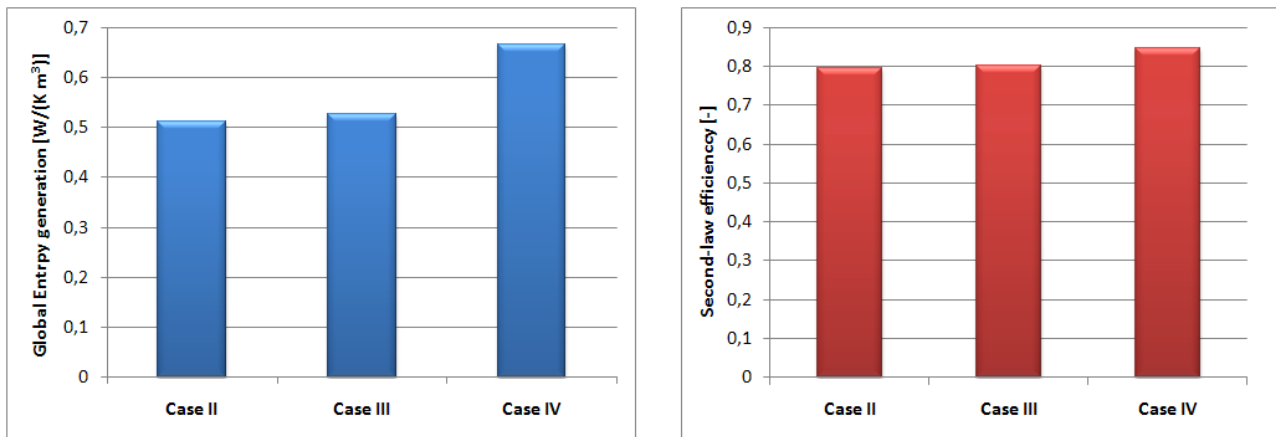


Figure 9. Entropy generation due to heat transfer. Case III and Case IV.



**Figure 10. Left) Heat release ratio  $\eta$ . Right) Entropy generation number  $N_s$ . Case II, III and IV.**



**Figure 11. Left) Global entropy generation. Right) Second-law efficiency.**

	PCM
Density $\rho$ [kg/m <sup>3</sup> ]	794
Thermal conductivity $k$ [W/(m K)]	0.2
Specific heat [J/(kg K)]	2300 (solid) 1800 (liquid)
Thermal expansion coefficient $\beta$ [1/K]	0.00091 [27]
Reference Temperature $T_0$	51
Melting temperature range [°C]	51– 56
Latent heat [kJ/kg]	249

Table 1. Thermophysical properties of the PCM (RT55) [20].

	number of fins	fins distribution	mass flow rate, $\dot{m}_{inlet}$ [kg/h]	Inlet temperature $T_{inlet}$ [°C]	Reynolds number, $Re$	Stefan Number, $Ste$
Case I	0	unfinned pipe	28.8	35	364	0.24
Case II	12	uniform	28.8	35	364	0.24
Case III	27	uniform	28.8	35	364	0.24
Case IV	27	non- uniform	28.8	35	364	0.24

Table 2. Computational cases studied.